Height control of laser metal-wire deposition based on iterative learning control and 3D scanning

Almir Heralić [a,c,*], Anna-Karin Christiansson [a], Bengt Lennartson [b]

[a] University West, Department of Engineering Science, SE-461 86 Trollhättan, Sweden
[b] Chalmers University of Technology, Department of Signal and Systems, SE-412 96 Göteborg, Sweden
[c] Volvo Aero Corporation, SE-461 81 Trollhättan, Sweden

ARTICLE INFO

ABSTRACT

Laser Metal-wire Deposition is an additive manufacturing technique for solid freeform fabrication of fully dense metal structures. The technique is based on robotized laser welding and wire filler material, and the structures are built up layer by layer. The deposition process is, however, sensitive to disturbances and thus requires continuous monitoring and adjustments. In this work a 3D scanning system is developed and integrated with the robot control system for automatic in-process control of the deposition. The goal is to ensure stable deposition, by means of choosing a correct offset of the robot in the vertical direction, and obtaining a flat surface, for each deposited layer. The deviations in the layer height are compensated by controlling the wire feed rate on next deposition layer, based on the 3D scanned data, by means of iterative learning control. The system is tested through deposition of bosses, which is expected to be a typical application for this technique in the manufacture of jet engine components. The results show that iterative learning control including 3D scanning is a suitable method for automatic deposition of such structures. This paper presents the equipment, the control strategy and demonstrates the proposed approach with practical experiments.

1. Introduction

Production of complex metal structures, by means of traditional manufacturing, often requires expensive precision castings or oversized forgings that need extensive machining. For large and complex structures that are manufactured in small quantities using high-cost materials, e.g. jet engine components, traditional methods lead to significant production costs, due to high scrap rates and long lead-times. Rapid manufacturing techniques based on additive layer manufacturing have therefore gained an increased attention due to their ability to fabricate fully dense metal shapes without the need of dies or extensive machining. If rapid manufacturing can be included as a supporting technique to traditional manufacturing methods, the production costs and lead-times can be decreased. The flexibility of rapid manufacturing can also allow for late design changes or repair of worn out parts. Moreover, the technique enables the use of other materials and new designs, utilizing, e.g. sheet metals, which can help to reduce the total weight of the final component.

Since their first introduction three decades ago, additive manufacturing techniques for metal have been developed and commercialized in the industry under names such as Direct Metal Deposition [1], Laser Engineered Net Shaping [2], Shaped Metal Deposition (SMD) [3], Selective Laser Melting [4], and Electron Beam Melting [5]. Apart from the SMD system, which utilizes metal wire, the parts are built from powderized feedstock either in a powder-feed process [1,2] or a powder-bed process [4,5]. The heat source used for melting the additive material is usually a high power laser, an electron beam or a tungsten inert gas (TIG) welding source. Traditionally, the powder based processes have been developed towards the manufacture of small and complex geometries with less focus on the deposition speed. For large structures with moderate complexity, such as flanges or bosses, it is more rewarding to use wire based techniques since these will give a better surface finish, could lead to better material quality, and also higher deposition rates [6,7]. The use of wire will also give better process efficiency and cleaner working environment since all wire that is fed into the melt pool is utilized, in comparison to a substantial amount of scattered powders that are not melted when currently available powder based techniques are used.

Basic process characteristics of wire-based additive manufacturing and material properties of deposited beads and 3D parts have been studied by many authors [3,8–20]. Combination of wire

and powder feeding has also been reported [21–23]. A conclusion can be drawn that a wire-based deposition process is sensitive to wire position and orientation relative to the melt pool and the deposition direction. Careful tuning of the wire feed rate, the heat input, and the travel speed are also important in order to obtain defect-free beads. Moreover, in [24] it is further argued that in order to achieve good process stability for multi layered deposition, continuous process monitoring and control of, e.g. the wire feed rate, is also necessary. In [25] a camera-based monitoring system is developed for closed loop control of straight-bead deposition and in [18] a temperature monitoring system is investigated for a laser metal-wire deposition process. However, apart from the mentioned references this subject has not yet been investigated to any great extent in the literature. By contrast, there are several publications on this subject for powder-based systems, e.g. monitoring and process control using cameras [26–28], closed-loop height control using photo diodes [29–32], powder flow control based on motion system speed profile [33], temperature measurements using pyrometers [34–36]. However, transferring these results to wire-based deposition systems is not a straightforward task since the two processes are dissimilar in many ways.

A robotized laser metal-wire deposition system has been developed at University West, Sweden, in close cooperation with Swedish industry. For this process a camera-based monitoring system and closed loop control of bead width and height has been developed and demonstrated for straight bead deposition [25]. The work presented in this paper is a continuation of that work. The main contribution is a generalized height controller based on iterative learning [37] that can cope with arbitrary deposition patterns. It uses height information from preceding layers, obtained by means of 3D scanning, and prevents the deterministic disturbances (which the controller learns during the deposition), and compensates for non-deterministic temporary disturbances. The result is a stable deposition process with small errors and low control activity. The material considered in this paper is Ti–6Al–4V deposited on plates of same material.

2. System hardware

The deposition system is a modified laser welding system consisting of a high power laser, a deposition tool, an industrial robot arm, an inert gas tent, a data acquisition system, an operator interface, and a control system.

The laser heat source is an IPG Photonics fiber laser with a maximum power of 6 kW. The use of a laser as a heat source is grateful since it gives low heat input into the substrate (compared, e.g. to a TIG heat source) leading to less residual stress and less deformation. The robot, which generates the movement of the tool relative to the substrate, is an ABB 4400 industrial robot arm with six degrees of freedom. The use of a robot enables high flexibility in terms of feasible geometries and objects that can be modified or repaired.

2.1. Deposition tool

The deposition tool consists of an optical system, which focuses the laser beam, a wire feeder, a laser scanner, and a camera. The optical system consists of a collimator and a focusing lens, which together generate a 1.5 mm wide spot in focus. However, since the chosen wire diameter is 1.2 mm the laser beam is defocused into a larger spot (roughly 3.6 mm on the deposition surface) in order to allow for a more flexible interaction between the wire tip and the melt pool. The focus point is placed below the surface in order to avoid plasma generation. Here, the choice of wire diameter is a matter of convenience. Other wire diameters are equally possible with proper choice of laser spot diameter. The wire feeder is a self-regulated push/pull feeding system from Fronius. A push mechanism is mounted at the wire spool and a smaller pull mechanism is mounted at the nozzle. This setup has a fast response and ensures good compliance with the desired wire feed rate at the nozzle. The tool is illustrated in Fig. 1.

2.1.1. Laser scanner

A laser scanner is utilized for the purpose of obtaining a 3D height profile of the manufactured part after each deposited layer. In this work a laser scanner from Micro-Epsilon (scanControl 2810-25) is used that operates according to the principle of optical triangulation. That is, a laser line is projected onto the target surface and the reflected light is captured by a two dimensional sensor from which a single-line height profile is calculated. Resolution of the scanner in the z-axis is specified to 10 µm. A 3D height profile is obtained by a relative movement between the scanner and the part in the x-direction (for coordinates see Fig. 1), generated by the robot, during which the scanner is triggered by an in-house developed software to perform measurements. The part is scanned with a speed of 5 mm/s, and each 50 ms a new profile is extracted. This results in 250 µm spatial resolution along the x-axis. At the currently chosen measurement distance (between the scanner and the part) the length of the laser line is around 35 mm. The maximum number of measurement points per scanned line is 1024, however, in order to limit the amount of information generated for each scanning, 256 points/line are used. A 35 mm wide laser line gives a spatial resolution of 140 µm along the y-axis.

During deposition it is important to protect the scanner from the high power laser reflections and the heat radiation from the built part. For this purpose, a linear drive unit, on which the scanner is mounted, is utilized such that it lifts the scanner away from the melt pool during the actual deposition, and lowers it
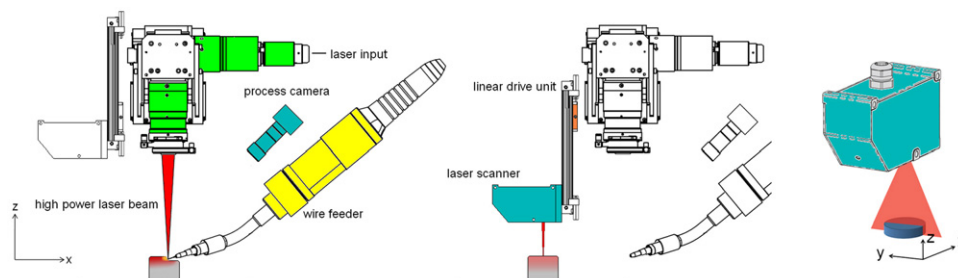

Fig. 1. Deposition tool with the laser scanner. Left, deposition mode; middle, scanning mode; right, coordinate axes during scanning.
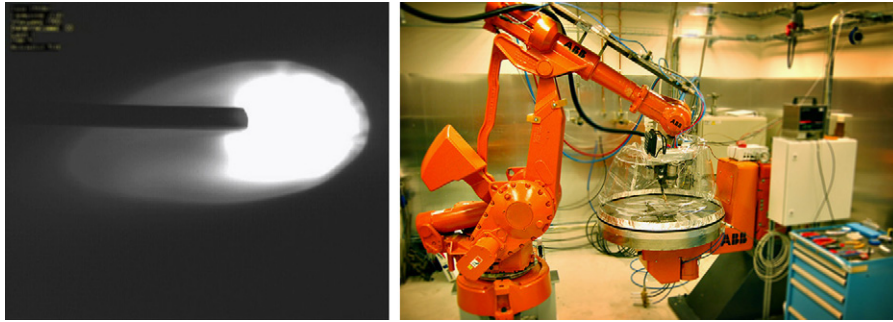
Fig. 2. Left, close-up image of the deposition process as seen by the process camera. Right, the deposition cell with the ABB robot and the protective inert gas tent.

down at the time of scanning, see Fig. 1. The repeatability of the linear drive unit in the z-direction is measured to $\leq 30\ \mu m$.

2.1.2. Process camera

A CMOS camera is mounted on the deposition tool in order for an operator to monitor the interaction between the wire tip and the melt pool during the deposition process. The visual feedback is meant to help the operator to evaluate the controller and to spot any disturbances that are not taken care of by the controller. The field of view is concentrated on a small area surrounding the melt pool. The high power laser is blocked by a filter placed in front of the camera's lens. Furthermore, due to the high brightness of the process, a small aperture and a short shutter time are chosen. This gives a good contrast of the details in the melt pool, but it also means that the surrounding is underexposed and thus black, see the left part of Fig. 2. Hence, for better results illumination is required, preferably by using well defined light sources such as xenon light sources or lasers, although not yet implemented in this work.

2.2. Oxygen sensor

During deposition of Ti alloys it is crucial to maintain the oxygen content below a certain threshold to minimize the oxidation of the built part. The deposition is therefore performed in a protective tent filled with inert gas. In order to monitor the oxygen content a thin tube is inserted inside the tent from which a small quantity of air is continuously pumped into an oxygen sensor for measurement. In this work argon is used as the inert gas.

2.3. User interface

The user interface is designed to provide an operator with all the necessary information needed to run the process remotely from outside the laser room. This is an important feature due to the potential risks associated with the use of high power lasers in general, and mounted on robots in particular. If necessary, the interface allows the user to make on-line changes of the laser power, the deposition speed, the wire feed rate, and the robot's height.

Two additional cameras are installed in order to give an overview of the process and the laser room. The scanned surface is also clearly displayed as well as the details of the height deviations for the last deposited layer.

2.4. Data acquisition

All data that is presented to the operator is also stored in a MySQL database with a timestamp. This enables easy access to the stored data and hence it allows for easy analysis of the experiments. Several flags are used, such as layer number, laser on/off, etc. which further

simplifies the extraction of the data of interest for post analysis. The sampling frequency in this work is 33 Hz.

3. Deposition procedure

The on-line controller is evaluated through deposition of bosses, i.e. knob-like parts with a size in the range of some cm in all directions. The target part is a 25 mm high circular cylinder with 30 mm diameter. The part is produced in the following way: The robot moves the deposition tool according to a pattern while the high power laser beam generates a melt pool on the substrate into which the wire is fed continuously. The wire is melted partially by the laser beam and partially by the heat from the melt pool, and upon solidification a bead is created. The beads are deposited side by side, according to the pattern, forming a layer with a desired contour. The deposition is then repeated for a sufficient number of layers until the desired height is obtained. Here, the part is generated by depositing 35 layers. The deposition pattern is an arithmetic spiral, i.e. the successive turnings of the spiral have a constant separation distance, see Fig. 3. This distance is chosen so that adjacent beads are overlapping in a way that the intermediate area gets as flat as possible.

In the open-loop case, for each new layer, the robot's tool center point (TCP) is offset by an estimated layer height in the z-direction, according to (1), where $\mathcal{T}_{j+1}^{z}$ is the tool's position on the z-axis at layer $j+1$, and $\hat{h}_l$ is the estimated layer height. The estimate $\hat{h}_l$ is based on practical experience and here chosen as constant over layers:

$$\mathcal{T}_{j+1}^{z} = \mathcal{T}_{j}^{z} + \hat{h}_l \tag{1}$$

In this work Ti–6Al–4V wire is deposited onto 3 mm plates of same material. The plates are mounted on a clamping fixture placed inside an inert gas tent. The oxygen level inside the tent is maintained below 100 ppm (parts per million) at all times during deposition. Between each layer the top surface of the part is scanned with the laser scanner described in Section 2.1.1. Since the chosen scanner is not intended for hot surfaces a pause of one minute is made after each deposited layer in order to minimize the scanning errors caused by the hot top surface of the part.

4. Control methodology

Multi-bead multi-layered deposition is a complex process that depends on several parameters such as the shape of the part, the choice of the deposition pattern, the heat input, the deposition speed, and the wire position- and orientation relative to the melt pool. These parameters affect the stability of the deposition process, the geometry of the final part, and its metallurgical properties. In this work the aim is to develop a controller that
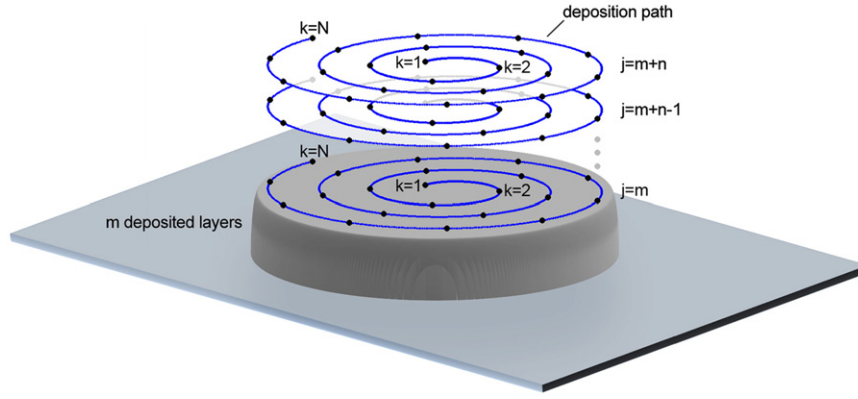
Fig. 3. Clarification of time index k and layer (iteration) index j. Note that the time is reset for each new layer.

ensures a smooth surface on each layer, given a set of predefined deposition parameters, and thereby guaranteeing a stable deposition. Potential metallurgical requirements are here assumed to be fulfilled given the set of nominal deposition parameters.

The control system is a combination of an iterative learning controller (ILC) for height deviations and a step-height compensator. The ILC is intended to smoothen out height deviations by controlling the wire feed rate while the step-height compensator should adjust the robot's TCP, in the z-direction, in order to compensate for incorrectly estimated layer height.

4.1. Iterative learning controller

During deposition the height variations within a layer are generated as a consequence of the chosen process parameters, e.g. the shape of the deposition pattern, and due to potential disturbances, e.g. in the wire feed rate. The dominating factor for causing height variations has shown to be the choice of process parameters. The resulting variations in height are deterministic, but the dependency is complex and hard to predict. For each new setting of process parameters the *a priori* knowledge of the resulting system's dynamics is therefore limited. Hence, the height controller should adapt to local process variations on-line. Since the deposition process is repeated, layer after layer, it can be seen as an iterative process with deposition layers as the iteration domain. It is therefore natural to choose the ILC structure for height control.

Iterative learning control was mathematically formalized three decades ago, see, e.g. the seminal works in [38,39] or a recent survey paper [37]. Traditionally, the ILC approach has been implemented for improving reference following in repetitive tasks, most often involving industrial robots, see, e.g. [40].

Before defining the ILC algorithm, a performance measure needs to be defined. Assume that the ILC algorithm operates on a set of N discrete points k (sampled with the sampling time T_s), which are uniformly distributed along the deposition path (see Fig. 3). Define $H_j(k)$ as the total height of the deposited part in a single point, i.e. at time index k, after layer j has been deposited, and $\mathcal{T}_j^z$ as the robot's height at layer j. Define then the mean layer height as

$$\overline{h}_j = \frac{1}{N} \sum_{\ell=1}^{N} (H_j(\ell) - \mathcal{T}_j^z) \tag{2}$$

where $H_j(k)$ is obtained using the 3D scanner described in Section 2.1.1. Using (2), define the performance measure, at each discrete
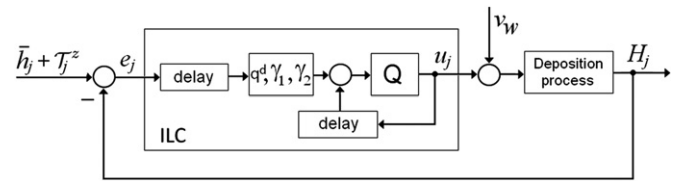

Fig. 4. ILC architecture as implemented in this work. The delay is in the iteration domain and v_w is the nominal wire feed rate.

point k, as the error

$$e_j(k) = \overline{h}_j + \mathcal{T}_j^z - H_j(k) = \frac{1}{N} \sum_{\ell=1}^{N} H_j(\ell) - H_j(k) \tag{3}$$

The error $e_j(k)$ thus measures the deposited part's height variations from a mean value, at each discrete point k, which should be minimized. By defining the error as the deviation of $(H_j(k) - \mathcal{T}_j^z)$ from its mean value $\overline{h}_j$, rather than from the estimated layer height $\hat{h}_l$, the ILC is limited to focus on height variations only, i.e. to achieve a flat surface. This will minimize the control action and thereby also the process induced disturbances, see Section 4.2 for further discussion.

Using (3) the ILC algorithm can now be defined. Here, a second order ILC is chosen such that it incorporates the error measurements from the previous two iterations, i.e. $e_j(k)$ and $e_{j-1}(k)$:

$$u_{j+1}(k) = Q(q_k)[u_j(k) + q_k^d(\gamma_1 e_j(k) + \gamma_2 e_{j-1}(k))] \tag{4}$$

where u_j is the control input that controls the wire feed rate on layer j, γ_i are the so called learning gains, and $Q(q_k)$, defined as the Q-filter, is a zero phase low pass filter based on a 2nd order Butterworth filter [41], in the time shift operator q_k ($q_k^{-1} u_j(k) = u_j(k-1)$). Furthermore, a time shift operator, q_k^d, acts on the two error signals, $e_j(k)$ and $e_{j-1}(k)$, where d denotes the number of samples the corresponding signal is shifted in time. Note that (4) is noncausal for $d > 0$. However, this gives no problems since the time shift is applied on error measurements from past iterations only, i.e. iterations for which a complete error signal is available. Note further that, for each new iteration, the time is reset as illustrated in Fig. 3. Fig. 4 shows the ILC architecture as implemented in this work.

The higher order ILC is needed since each new layer is deposited on top of its preceding layer, and not on a new flat substrate. Hence, the error is inherited, and thus accumulated, from previous iterations. Due to this feature, the ILC controlled deposition system becomes unstable if a first order ILC is used.
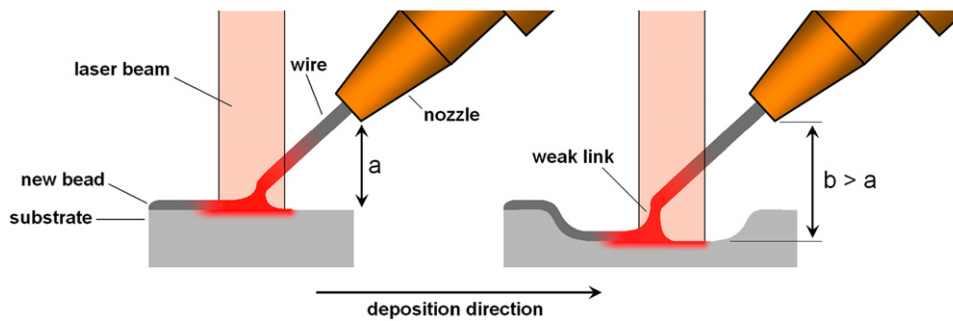
Fig. 5. Illustration on how the path of the wire traveling through the laser beam is increased when the distance between the nozzle and the substrate is increased.

4.2. Step-height compensator for increased stability

In order to ensure stable deposition during wire based metal deposition, it is crucial that the wire nozzle position and angle relative to the top surface of the melt pool is maintained as constant as possible. If there is a deviation from the nominal position, between the nozzle and the melt pool, e.g. due to large height deviations within a layer, errors such as globular transfer of the molten wire or insufficient melting of the wire are likely to occur [24]. The position and angle of the nozzle determine the distance, i.e. the time, between where the wire tip enters the laser beam and where it later enters the melt pool, see Fig. 5. Assuming constant laser power and wire feed rate, altering this distance will alter the amount of energy that is transferred to the wire tip before it reaches the melt pool. Too much energy and the wire tip will melt too early, forming droplets of molten wire rather than a continuous transfer between the wire tip and the melt pool. That is, the "weak link" in the right side of Fig. 5 expands before it finally breaks when the surface tension forces become too weak. Too little energy and the wire tip will instead enter the melt pool still solid, and thereby increasing the risk of lack-of-fusion defects.

Defects caused by insufficient melting of the wire have a significant impact on the deposited part's fatigue life and are therefore not accepted in most relevant applications. Globular transfer of the molten wire has not been found to affect the deposited part's metallurgical properties, but can lead to huge irregularities in the bead height. Such irregularities usually get self-amplified (if not compensated for at an early stage), by causing further instability on the subsequent layers. Once the irregularities have grown in amplitude, the high level of wire feed rate, needed to compensate for the deviations, might lead to insufficient melting of the wire, and ultimately lack-of-fusion defects.

Towards ensuring stability (in addition to the height ILC), the step height of the robot can also be adjusted to fit the current height of the deposited part. Recall that in (1) the robot's TCP height in the open-loop case is updated by an estimated layer height $\hat{h}_l$, which is assumed constant. However, the real layer height is known to vary slightly as a function of layers (when deposition parameters are constant). The variations are most dominant during the initial layers, after which a steady state is usually reached. Hence, if the robot's offset is updated in relation to the mean height of the latest deposited layer, rather than a constant estimate, the distance between the wire tip and the melt pool will remain close to its nominal value, throughout the deposition. Approaching final layers, the total height of the part should, however, be revised in respect to the desired dimensions and, if necessary, the total number of layers can be adjusted.

The step-height compensator is defined in the following way: After each scanning, the mean layer height, $\overline{h}_j$, is obtained according to (2). The robot's TCP is then offset in the z-direction

by $\overline{h}_j$, according to the following equation:

$$\mathcal{T}_{j+1}^z = \mathcal{T}_j^z + \overline{h}_j \tag{5}$$

For clarity, the deposition process' different steps are here summarized:

1. Time index k is reset when a new layer is to be built.
2. Layer j is deposited using the control action u_j.
3. Total height of the part H_j is scanned.
4. Mean layer height $\overline{h}_j$ is calculated using (2).
5. Error e_j is obtained using (3).
6. New control action u_{j+1} is calculated using (4).
7. Robot's new height position $\mathcal{T}_{j+1}^z$ is updated using (5).
8. Index j is incremented and the process is repeated.

5. System description and modeling for control

In this section a combined time- and iteration domain system description is developed, both for plant- and learning dynamics. A stability criterion is also defined, which is later used for parameter tuning in Section 6.

5.1. Plant dynamics

In the time domain, the plant dynamics is investigated in terms of height change as a function of Δv_w (deviation around the nominal wire feed rate v_w) and time. This is done by a step response experiment, i.e. the input signal, the wire feed rate, is perturbed during single bead-on-plate deposition, and the output, the deviation from a nominal bead height, as a function of time, is measured. The perturbation is a positive step change, and the process output is analyzed by observing the shape of the response, from which features such as the time constant and the gain of the plant can be extracted. The result from the step response experiment is illustrated in Fig. 6. It shows that the process exhibits second order dynamics. The time delay appears to be negative, i.e. it appears as if the system responds slightly before the actual change in the input signal. This is due to the fact that the melt pool has a distribution in space and, due to internal fluid flows, any change in added mass is distributed across the entire melt pool.

The resulting smoothing effect can be considered as a low pass filter in the time domain and means that a change in added mass, at a certain point on the deposition path, affects the height at previous points on the path as well. When the solidified bead is scanned, it will then appear as if the response to the change in added mass has started earlier than the input change itself. Therefore, the non-causal response, observed in Fig. 6, will be approximated with a first order system with a zero phase low pass filter. Details regarding zero phaser filters can be found in [41]. The zero phase characteristics are here important in order to
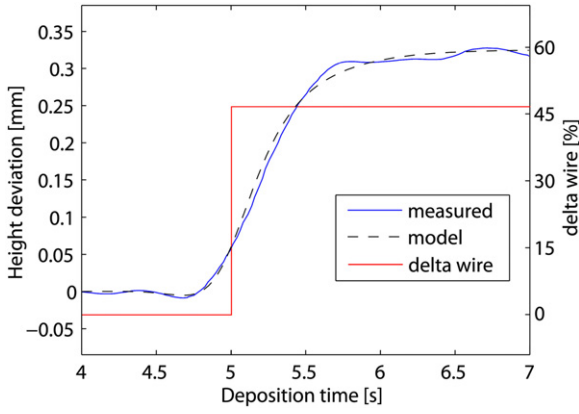
Fig. 6. Height response (solid line, scanned after solidification) due to a step change in wire feed rate compared to the simulated response (dashed line).

allow for high frequency attenuation without introducing lag. The transfer function, $G_{wh}(s)$, of the first order approximation from the wire feed rate to the bead height, is given in the following equation:

$$G_{wh}(s) = \frac{K_{wh}}{1 + sT_{wh}} \tag{6}$$

where, K_{wh} is the static gain and T_{wh} is the system's time constant. Note that the low pass characteristics is added first in (9). The static gain is defined as the ratio between a change in the output (the steady state value) and the change in the input signal, given that the process had previously reached a steady state before the time of the input change. The time constant is defined as the time at which the step response has reached 63% of its final value minus the time delay (which in this case is set to zero). For the chosen process parameters, T_{wh} is estimated to 0.37 s. For further details regarding transfer function estimation through step response experiments, see, e.g. [42]. Note that the transfer function $G_{wh}(s)$ regards the deposition process as being a single straight bead and hence, it does not model the complex interaction between adjacent beads. In discrete time, sampled with T_s, (6) becomes

$$y(k+1) = a_d y(k) + b_d u(k) \tag{7}$$

where y is the output height, $a_d = e^{-T_s/T_{wh}}$, $b_d = K_{wh}(1 - e^{-T_s/T_{wh}})$, and u is the control input (wire feed rate). The difference equation in (7) assumes a single bead deposited on a flat surface without disturbances. In order to incorporate the previous layers' height deviations and load disturbance, (7) is augmented according to the following equation:

$$x_j(k+1) = a_d x_j(k) + b_d u_j(k) + v(k)$$
$$y_j(k) = x_j(k) + y_{j-1}(k) \tag{8}$$

where j is the iteration index, $x(k)$ is a state variable, and v is a deterministic load disturbance that appears in every iteration and is same for each layer. That is, v is a function of time k, such that $v_j(k) = v_{j+1}(k)$, $\forall j,k$. Here, u_j, v_j, x_j, and y_j are N-sample sequences as follows:

$$u_j(k), \quad k \in \{0,1,\ldots,N-1\}$$

$$v_j(k), \quad k \in \{0,1,\ldots,N-1\}$$

$$x_j(k), \quad k \in \{1,2,\ldots,N\}$$

$$y_j(k), \quad k \in \{1,2,\ldots,N\}$$

where the state variable $x_j(0) = 0$, $\forall j$. By iterating (8), it is straightforward to obtain the lifted system representation, which gives a combined time- and iteration domain dynamics of the plant (9). The representation in the following equation is used for stability analysis in Section 6:

$$\underbrace{\begin{bmatrix} y_{j+1}(1) \\ y_{j+1}(2) \\ \vdots \\ y_{j+1}(N) \end{bmatrix}}_{\mathbf{y}_{j+1}} = \mathbf{H}_{LP} \underbrace{\begin{bmatrix} b_d & 0 & \cdots & 0 \\ a_d b_d & b_d & \cdots & 0 \\ \vdots & \vdots & \ddots & \vdots \\ a_d^{N-1} b_d & a_d^{N-2} b_d & \cdots & b_d \end{bmatrix}}_{\mathbf{P}} \underbrace{\begin{bmatrix} u_{j+1}(0) \\ u_{j+1}(1) \\ \vdots \\ u_{j+1}(N-1) \end{bmatrix}}_{\mathbf{u}_{j+1}}$$

$$+ \underbrace{\begin{bmatrix} y_j(1) \\ y_j(2) \\ \vdots \\ y_j(N) \end{bmatrix}}_{\mathbf{y}_j} + \underbrace{\begin{bmatrix} 1 & 0 & \cdots & 0 \\ a_d & 1 & \cdots & 0 \\ \vdots & \vdots & \ddots & \vdots \\ a_d^{N-1} & a_d^{N-2} & \cdots & 1 \end{bmatrix}}_{\mathbf{D}} \underbrace{\begin{bmatrix} v(0) \\ v(1) \\ \vdots \\ v(N-1) \end{bmatrix}}_{\mathbf{v}} \tag{9}$$

In (9), $\mathbf{H}_{LP}$ is the low pass filter discussed earlier in this section. Without the zero phase characteristics, $\mathbf{H}_{LP}$ introduces an unrealistic lag, which is quickly amplified since the height deviations from preceding layers are accumulated.

The basis of the filter is a 2nd order Butterworth low pass filter. Assume that the discrete time state-space representation of the filter is given as

$$z(k+1) = A_f z(k) + B_f g(k)$$
$$f(k) = C_f z(k) + D_f g(k) \tag{10}$$

where g represents the input signal, z the state vector, and f the filtered signal. In order to obtain zero-phase filtering, the input signal is processed through the filter in (10), after which the output is time-reversed and processed by the same filter, once again. The procedure is thus non-causal and requires a finite length input signal. However, the signals which are processed by $\mathbf{H}_{LP}$ in (9) are all based on past inputs and outputs, and hence, the causality requirements can be relaxed.

To obtain a static representation of $\mathbf{H}_{LP}$, an $N \times N$ H_{LP}^*-matrix is formed:

$$H_{LP}^* = \begin{bmatrix} D_f & 0 & 0 & \cdots & 0 \\ C_f B_f & D_f & 0 & \cdots & 0 \\ C_f A_f B_f & C_f B_f & D_f & \cdots & 0 \\ \vdots & \vdots & \ddots & \ddots & \\ C_f A_f^{N-2} B_f & C_f A_f^{N-3} B_f & \cdots & C_f B_f & D_f \end{bmatrix} \tag{11}$$

where N is the length of the input signal. The final zero-phase $\mathbf{H}_{LP}$ matrix is obtained by multiplying a transformed H_{LP}^*-matrix with itself according to

$$\mathbf{H}_{LP} = (T H_{LP}^* T) H_{LP}^* \tag{12}$$

where T is an anti-diagonal identity matrix

$$T = \begin{bmatrix} 0 & \cdots & 0 & 1 \\ 0 & \cdots & 1 & 0 \\ \vdots & \ddots & \vdots & \vdots \\ 1 & \cdots & 0 & 0 \end{bmatrix}$$

Here, a cut-off frequency of 1 Hz is chosen. The low cut-off frequency reflects the strong smoothing effect that the melt pool has on the final bead shape. The simulated step response of the lifted system in (9) is compared to the measured step response in Fig. 6.
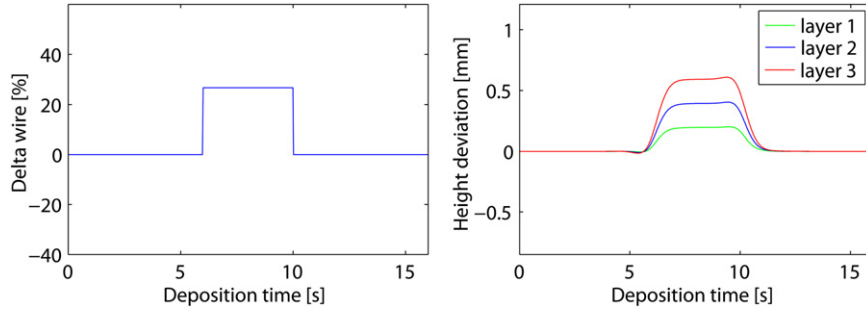
Fig. 7. Left, recurring pulse disturbance used for simulated evaluation of the ILC system. Right, resulting simulated height deviation when the controller is turned off.

5.2. Learning dynamics

Using (9), a combined time- and iteration domain representation of the learning algorithm, given in (4), is derived. Since the plant in (9) models the height deviations from a flat surface (and not the real height of the component), the error e_j is here set as $e_j = -y_j$. Using this error formulation, the learning equation in (4) can be formulated as follows:

$$\mathbf{u}_{j+1} = \mathbf{Q}[\mathbf{u}_j - q_k^d(\gamma_1 \mathbf{y}_j + \gamma_2 \mathbf{y}_{j-1})] \tag{13}$$

where $\mathbf{u}_i$ and $\mathbf{y}_i$ are vectors of time signals u_i and y_i, respectively, containing all values of k, cf. (9). The Q-filter matrix $\mathbf{Q}$ is a static representation matrix of the Q-filter, derived from its state space model. The bandwidth of the Q-filter determines how large part of the disturbance dynamics should be learned. Here, the focus is on the low frequency characteristics of the process, and hence a low pass Q-filter is chosen. It has been shown that introducing a low pass Q-filter increases the robustness of the process, however, at the price of performance [43]. The filter is designed as a zero-phase digital filter, i.e. in the same way as $\mathbf{H}_{LP}$, in order to allow for high frequency attenuation without introducing lag.

5.3. Combined system representation

In order to analyze the stability of an ILC system it is often sufficient to investigate the stability of the learning dynamics [44]. However, since the plant output of the considered process depends directly on the previous outputs as well, an investigation of a combined plant- and learning dynamics system is instead required. To obtain such a system, (9) and (13) are combined and rewritten into a descriptor representation as follows:

$$\underbrace{\begin{bmatrix} I & 0 & -\mathbf{H}_{LP}\mathbf{P} \\ 0 & I & 0 \\ 0 & 0 & I \end{bmatrix}}_{E} \begin{bmatrix} \mathbf{y}_{j+1} \\ \mathbf{y}_j \\ \mathbf{u}_{j+1} \end{bmatrix} = \begin{bmatrix} \mathbf{H}_{LP} & 0 & 0 \\ I & 0 & 0 \\ -\mathbf{Q}q_k^d\gamma_1 & -\mathbf{Q}q_k^d\gamma_2 & \mathbf{Q} \end{bmatrix} \begin{bmatrix} \mathbf{y}_j \\ \mathbf{y}_{j-1} \\ \mathbf{u}_j \end{bmatrix}$$

$$+ \begin{bmatrix} \mathbf{H}_{LP}\mathbf{D} \\ 0 \\ 0 \end{bmatrix} \mathbf{v}$$

where I is an identity matrix. The descriptor matrix E in the above expression is eliminated from the left hand side, by multiplying the expression with E^{-1}, to obtain the following:

$$\begin{bmatrix} \mathbf{y}_{j+1} \\ \mathbf{y}_j \\ \mathbf{u}_{j+1} \end{bmatrix} = \underbrace{\begin{bmatrix} \mathbf{H}_{LP}(I-\mathbf{P}F_1) & -\mathbf{H}_{LP}\mathbf{P}F_2 & \mathbf{H}_{LP}\mathbf{P}\mathbf{Q} \\ I & 0 & 0 \\ -F_1 & -F_2 & \mathbf{Q} \end{bmatrix}}_{F} \begin{bmatrix} \mathbf{y}_j \\ \mathbf{y}_{j-1} \\ \mathbf{u}_j \end{bmatrix} + \begin{bmatrix} \mathbf{H}_{LP}\mathbf{D} \\ 0 \\ 0 \end{bmatrix} \mathbf{v}$$

$$\tag{14}$$

where $\mathbf{F}$ is the system matrix that is used for stability analysis in Section 6, and $F_1 = \mathbf{Q}q_k^d\gamma_1$ and $F_2 = \mathbf{Q}q_k^d\gamma_2$.

5.4. Stability definition

Stability is a central property for a control system. When a process is controlled using ILC, typically two questions are of interest namely, whether the error will approach zero as the number of iterations grow and, if the error does not approach zero, is it bounded? The way the error decays is also of interest, e.g. does it decay monotonically? Given the simplicity of the controller (i.e. no a priori knowledge of the system) and the additive nature of the process in the iteration domain, requirement such as monotonous error decay is presumably too demanding. Here, asymptotic stability is investigated. Define the spectral radius of a matrix M as follows:

$$\rho(M) = \max_{i=1,\dots,n} |\lambda_i(M)|$$

where $\lambda_i(M)$ is the ith eigenvalue of the matrix $M \in \mathbb{R}^{n \times n}$. The ILC system in (14) is asymptotically stable if the spectral radius [44]

$$\rho(\mathbf{F}) < 1 \tag{15}$$

where $\mathbf{F}$ is obtained from (14). Note that ensuring asymptotic stability does not guarantee a zero error. To investigate the error decay, the process is simulated using (14) in connection with tuning of the ILC parameters in the next section.

6. Parameter tuning using simulation

The ILC algorithm defined in (13) has four parameters that need to be decided; the learning gains, γ_1 and γ_2, the cut-off frequency of the Q-filter, and the time shift q_k^d. The aim is to ensure asymptotic stability of the system, i.e. to fulfill (15), and, if possible, monotonic error decay after short initial transients. However, the tuning of the controller parameters should also reflect some process characteristics which are not captured by the models described earlier. One example is the fact that fast and large wire speed variations might lead to deposition disturbances, such as globular transfer of the molten wire, as discussed in Section 4.2. At current state, automatic detection of the globular state and a suitable recovery action has not yet been developed. Hence, in this work the controller should perform in a way that minimizes the risk of this event. This is done by choosing controller parameters that give a slower response, i.e. lower control activity.

6.1. Learning gain

The tuning is based on the system described in (14). To begin with, $\mathbf{Q} = 1$ and $d = 0$ ($q_k^d = 1$), and various learning gain combinations, (γ_1, γ_2), are tested. The idea is to find a suitable and stable

(γ_1, γ_2) pair, after which an appropriate Q-filter is added to increase the robustness. The stability criterion (15) is investigated and the system is simulated for a number of iterations, where a recurring pulse disturbance is introduced at the same location for each layer. Fig. 7 shows the response of the pulse disturbance when no control activity is used, i.e. the deviation adds for each layer.

The learning gains are based on the static gain K_{wh} of the time domain plant. More specifically, γ_1 is chosen as the inverse of K_{wh} multiplied with a constant ($\overline{\gamma}_1$), while γ_2 is chosen proportional to γ_1, i.e.

$$\gamma_1 = \overline{\gamma}_1 / K_{wh}, \overline{\gamma}_1 > 0$$

$$\gamma_2 = -\overline{\gamma}_2 \gamma_1, \overline{\gamma}_2 > 0 \tag{16}$$

With its negative sign, γ_2 acts as a damping factor to the response of the controller, such that it suppresses the overshoot and subsequent oscillations that follow a fast initial response, due to γ_1. In order for the control signal to converge, $\overline{\gamma}_2$ should be chosen less than unity. Furthermore, stability analysis shows that if γ_2 is set to zero, the process becomes unstable for any value of γ_1, i.e. $\rho(\mathbf{F})|_{\gamma_2 = 0} > 1$. Hence, a higher order ILC structure (in the iteration domain) appears necessary for the current process. However, the analysis also indicates that, when both γ_1 and γ_2 are nonzero (and $\mathbf{Q} = 1$ and $d = 0$) the $\rho(\mathbf{F}) = 1$ at best, i.e. the system is only marginally stable. Thus, in order to ensure stability using the current ILC structure for the proposed plant model, it is necessary to use a Q-filter (which increases the robustness at the cost of performance [43]).

A set of different (γ_1, γ_2) are simulated and the root mean square (RMS) error between the resulting height deviations and a flat surface is investigated. For clarity, only a subset of these (γ_1, γ_2) combinations' RMS error is plotted in Fig. 8. The graphs on

the right side in Fig. 8 show the ratio between the control input and the disturbance, at time $t = 8$ s, i.e. during the disturbance shown in Fig. 7.

Based on simulation results, the marginally stable controller, obtained using $\gamma_1 = 1/K_{wh}$ and $\gamma_2 = -3/4\gamma_1$, i.e. with $\overline{\gamma}_1 = 1$ and $\overline{\gamma}_2 = 3/4$, are chosen for further investigation, see Fig. 8. This combination is a compromise between a reasonable response time and moderate control signal activity.

6.2. Q-filter and time shift operator

In order to increase the robustness of the ILC system, a low pass Q-filter is implemented. Fig. 9 shows the simulation results for three different cut-off frequencies ($f_c(\mathbf{Q})$), 0.5, 1, and 8 Hz. Here, $T_s = 0.03$ s, which corresponds to the real system's sampling time, and gives a Nyquist frequency of 16 Hz. The filter is evaluated for learning gains $\gamma_1 = 1/K_{wh}$ and $\gamma_2 = -3/4\gamma_1$, using the same evaluation procedure as in the previous section. When $f_c(\mathbf{Q})$ is set to 8 Hz, the spectral radius $\rho(\mathbf{F})$ is only marginally less than unity. With $f_c(\mathbf{Q})$ set to 0.5 and 1 Hz, a stable system is obtained with $\rho(\mathbf{F}) < 0.8$. From these results, $f_c(\mathbf{Q}) = 1$ Hz is chosen as a trade-off between robustness and response time. For cut-off frequencies below 0.5 Hz, $\rho(\mathbf{F})$ goes towards unity as $f_c(\mathbf{Q})$ is decreased.

In ILC related problems, the time shift q_k^d is often used to compensate for the time delay of the plant (usually one sample). Since the time delay is modeled as zero in this work, the question arise whether q_k^d can still improve the performance of the ILC in the transient regions. A set of simulation trials has been performed and results show that introducing a positive time shift q_k^d can make the eigenvalues move towards the origin. However, the eigenvalue displacement turns out to be only marginal, wherefore the results are not further elaborated here. The conclusion,
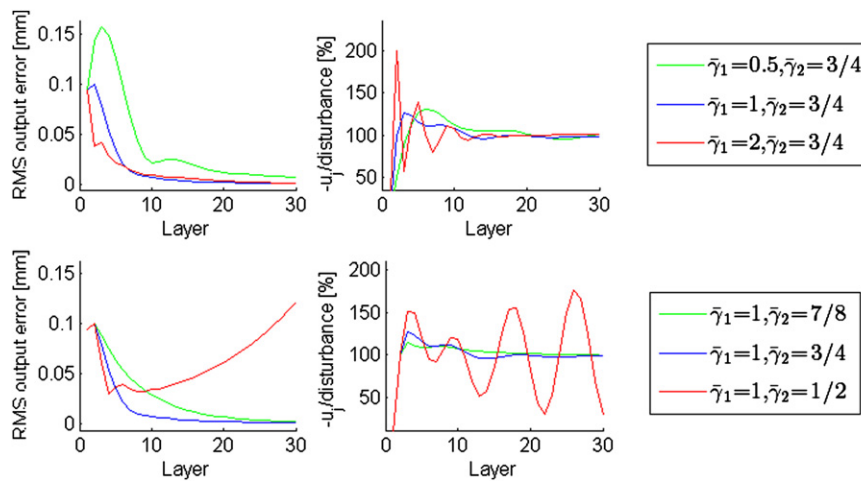

Fig. 8. Left, simulated RMS output error for a set of learning gains. Right, ratio between the control input and the disturbance, measured at $t = 8$ s.
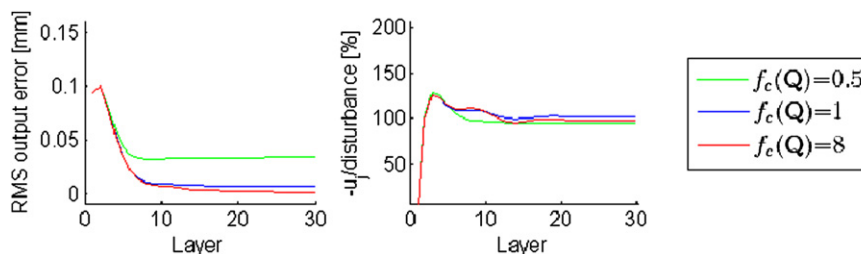

Fig. 9. Left, simulated RMS output error for three different Q-filters, using $\gamma_1 = 1/K_{wh}$ and $\gamma_2 = -3/4\gamma_1$. Right, ratio between the control input and the disturbance, measured at $t = 8$ s.

however, is that a time shift around the time constant of the plant ($d = \lceil T_{wh}/T_s \rceil$) appears to be a good choice for the considered plant model. By including a positive time shift (i.e. $d > 0$), a prediction of the error in the time domain is introduced. This helps the controller to react slightly in advance which can somewhat decrease the resulting height deviation.

7. Results and discussion

In this section the ILC system is compared with the open-loop system using experimental results. Control parameters derived in the previous section are used, i.e. $\gamma_1 = 1/K_{wh}$, $\gamma_2 = -3/4\gamma_1$, $f_c(\mathbf{Q}) = 1$ Hz, and $d = \lceil T_{wh}/T_s \rceil$.

7.1. ILC vs open-loop

A circular cylinder is chosen as the target. The controlled part was deposited for 35 layers, while the open-loop trial was aborted after 10 layers due to an increasing height error. The final height deviation of the open-loop deposited part is compared with the height deviation of layer 10 and 35 of the controlled part in Fig. 10. The open-loop curve shows that there are some areas where the height deviation increases rapidly, although the process parameters are constant throughout the deposition. Nevertheless, Fig. 10 further
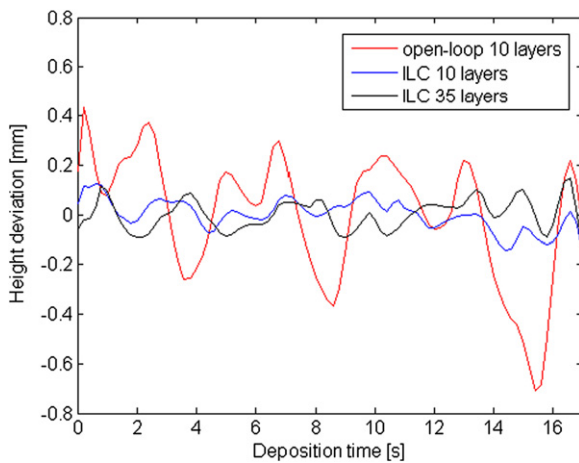

Fig. 10. Deviation from a mean layer height as a function of deposition time (i.e. along the deposition path). Comparison between the open-loop process and the ILC controlled process.
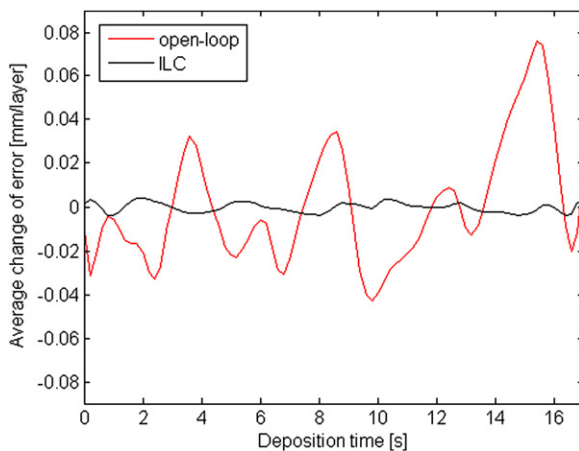

Fig. 11. Average rate of change of $e_j(k)$ (mm/layer) as a function of deposition time.

shows that the ILC algorithm is able to suppress these deviations and maintain a flat surface in a successful way.

In Fig. 11 the average rate of change of the error is shown. The curves are obtained in the following way. For each time unit k, a straight line is fitted to the corresponding errors, as a function of all deposited layers, and the slopes of each linear approximation (i.e. for all k) are obtained. These values represent the average rate of change of the error, i.e. in mm/layer. The ILC curve in Fig. 11 indicates that the control algorithm is able to restrain the height error throughout the deposition. This demonstrates the ILC algorithm's ability to learn the traits of a specific part, on-line without any *a priori* knowledge of the deterministic disturbances.

7.2. Step-height compensation

During the deposition of the controlled part the mean layer height $\overline{h}_j$, by which the robot's TCP is updated in the z-direction (5), is recorded. It is here compared to the estimated (and constant) layer height $\hat{h}_l$ used in the open-loop case. The accumulated difference, $\sum_{i=1}^{j}(\overline{h}_i - \hat{h}_l)$, is plotted in Fig. 12. It shows that, for the first 6 layers, the estimated layer height corresponds well to the real height. However, for the subsequent layers the real layer height is constantly higher than the estimate.

Here, the deviation is approximately 10% of the estimated layer height. However, the average deposition rate per layer, which is related to the control action, is close to the nominal value. This is illustrated in Fig. 13 where the average delta wire, Δv_w, is plotted, both as a function of layer and time. Δv_w corresponds to the control signal u_j, and in Fig. 13 it is represented as a deviation from the nominal wire feed rate (in [%]). Based on the average control action shown in Fig. 13, it can be argued that the error in the estimated height is presumably a result of a decreasing diameter of the component (see the right part of Fig. 14). A smaller diameter leads to higher layer height since the deposition rate is unchanged. The change of diameter is thought to be a result of surface tension forces in combination with changed absorbtion condition of the laser light for the contour bead (due to rounded edges).

Due to the error in the estimate $\hat{h}_l$, the distance between the wire nozzle and the melt pool, in the open-loop case, will constantly increase as of layer 6. Now recall the discussion in Section 4.2 and Fig. 5 and note that, a continuous increase in the distance between the wire nozzle and the melt pool will quickly lead to process disturbances such as globular transfer. Hence, if
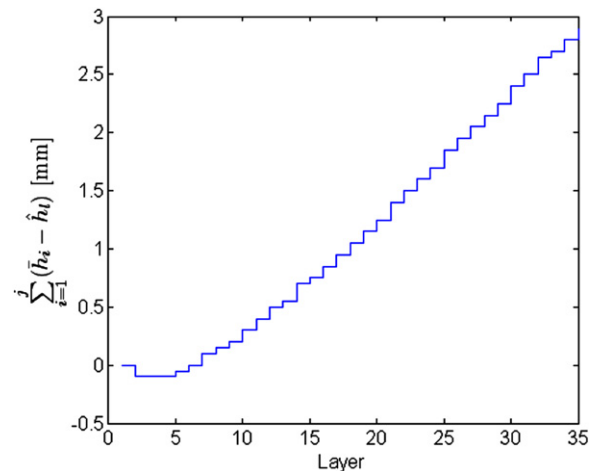

Fig. 12. Accumulated difference between real layer height $\overline{h}_j$ and a constant estimate $\hat{h}_l$ for the ILC controlled part. For the first 6 layers the estimated layer height corresponds well to the real value.
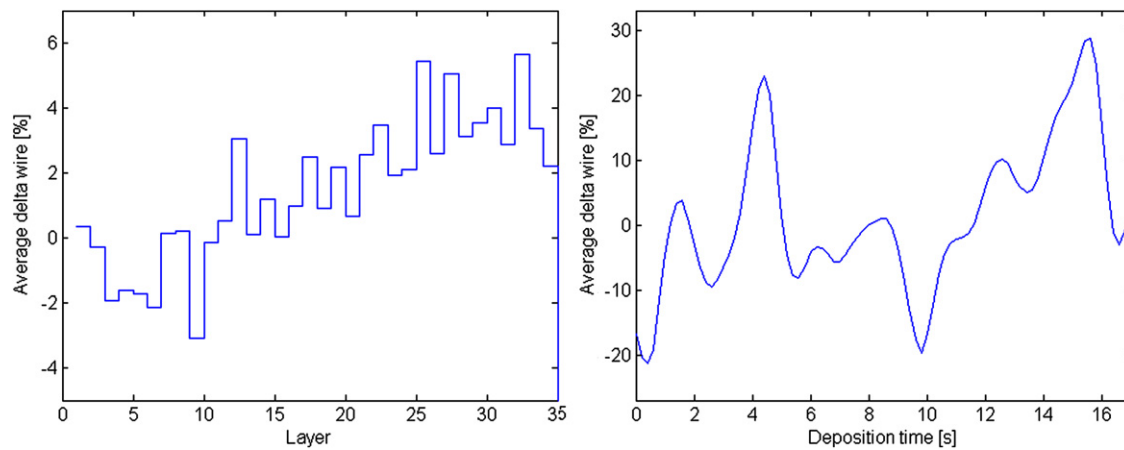
Fig. 13. Average of delta wire (Δv_w), i.e. average of the control signal, calculated for each layer j (left), and for each time instant k (right). Δv_w is here represented as the deviation from the nominal wire feed rate (in %).

Fig. 14. Circular cylinder deposited using iterative learning control.

the deposition process is run in the open-loop mode, it is important to have a set of estimates, or a function, that properly describe the evolution of the layer height for the intended part. The final part is depicted in Fig. 14. Note the somewhat wider diameter at the bottom layers.

7.3. Scanner related issues

The scanner used in this work (scanControl 2810-25) is a "general purpose" scanner, and as such not intended for scanning of hot metal surfaces. Nevertheless, it has a good measurement accuracy for the intended task if the surface of the deposited part is allowed to cool slightly. The scanner has some difficulties to obtain reliable measurements of the contour bead since the combination of shiny surface, rounded edges, and a low-power scanner laser results in a low amount of reflected light back to the scanner sensor. An example of a 3D profile obtained with the developed measurement system is shown in Fig. 15. The surface is overlaid with the deposition path of the robot. The figure shows that the outer contour bead's height is not correctly extracted in all regions. Because of this, the outer contour bead is deposited with nominal process parameters even in the controlled case, i.e. the ILC is turned off when the melt pool reaches the contour bead.

Possible improvements to this problem might include a more powerful scanner laser, optimized angle of incidence, or/and automatic adjustment of the sensor's exposure time for each individual point on the scanned line. In production, the cooling time between the layers must sometimes be kept at a minimum, which puts a demand on the scanner's ability to also scan hot surfaces.

7.4. Future work

The work presented in this paper is at an early stage towards the development of a robust and automatic process controller for laser metal wire deposition. Naturally, several issues are observed which have not yet been addressed.

In Section 4.2 the importance of keeping the distance between the wire nozzle and the melt pool is discussed. The update rule of the robot's TCP in (5) desires to keep this distance as constant as possible, but since the offset calculation is based on (and acts on) the entire deposition path, i.e. the mean layer height, local deviations might be rather high. A natural expansion of this approach is therefore to allow for continuous adjustments of the TCP value, along the deposition path, which are based on the local height deviations. Even so, process disturbances in terms of globular transfer of the molten wire might occasionally occur (e.g. on problematic contour beads). A robust automatic detection of the globular state, and a suitable recovery action, should therefore also be developed.

The scanner used in this work is for general purposes and is therefore not optimized for scanning of bright and hot metal surfaces. However, this is generally a major issue in the imaging/scanning society regardless the sensor used. Finding an appropriate sensor or a scanning procedure may therefore prove difficult. This will primarily affect the ability to obtain a correct representation of the outer contour beads. Hence, finding a way to estimate the reliability of the scanning information, and/or a way to estimate the control action for the outer contour bead based on information from the adjacent beads, are two interesting routes which should be investigated.

In Section 6.1 the current ILC structure shows some stability problems which are solved by using a Q-filter that increases the
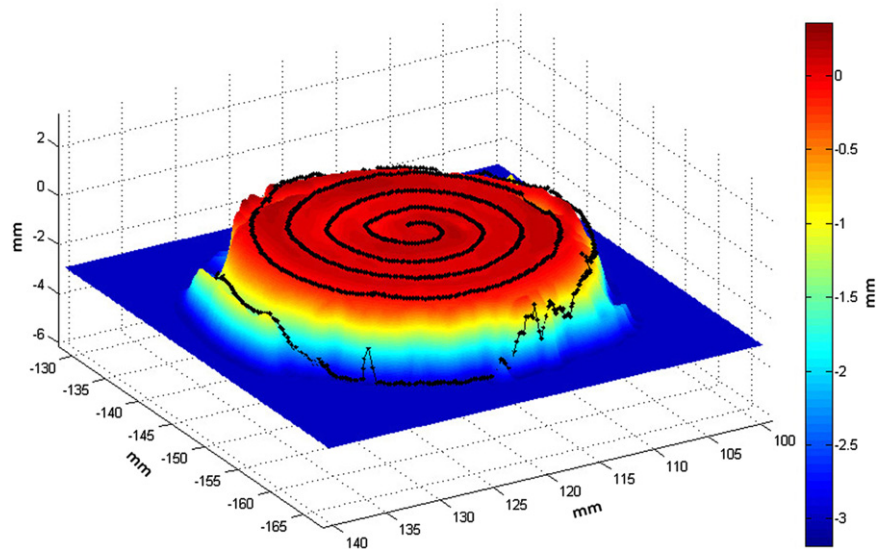
Fig. 15. An example of a scanned surface obtained with the developed measurement system. The black line shows the deposition path overlaid on the surface. The rounded edges of the outer contour bead are falsely reproduced.

robustness at a price of performance. A natural continuation is therefore to investigate other ILC structures, e.g. a higher order in the time domain, and related stability properties.

8. Conclusion

A laser metal wire deposition cell has been built up at University West with a monitoring system, featuring cameras and a 3D scanner. The monitoring system enables on-line visual feedback, both of the process and the deposited layer's topological profile.

Use of a scanner to produce 3D images of each layer gives a good insight into the process-induced disturbances and thus enables control of the process. This information can also be a valuable input for future modeling and simulation, or for development of Off-Line Programming tools. The structure of the measurement system allows for synchronized storage of all measured data into a database, which simplifies the extraction and the analysis of the experimental data.

Using the developed monitoring system an *in-process* height controller has been developed and demonstrated. The control algorithm is based on iterative learning. The control signal adjusts the wire feed rate based on 3D scanned data of the deposited part. The results show that the developed ILC is able to learn the traits of a specific part on-line without any *a priori* knowledge of the deterministic disturbances. This is important since deposition of several adjacent beads within a layer generate height variations which depend on the chosen parameters in a complex way, and are therefore hard to predict. The controller is thereby able to compensate for local changes and maintain a smooth flat surface throughout the deposition. The experimental work is conducted using Ti–6Al–4V, but the results can be generalized to other materials as well. Furthermore, the controller is useful for arbitrary components and deposition patterns, while the scanner is mainly intended for small-size bosses.

Acknowledgments

References

[1] Mazumder J, Koch J, Nagarthnam J, Choi J. Rapid manufacturing by laser aided direct deposition of metals. Adv Powder Metall Part Mater 1996;4(15):107–118.

[2] Atwood C, Griffith M, Schlienger M, Harwell L, Ensz M, Keicher D, et al. Laser engineered net shaping (LENS): a tool for direct fabrication of metal parts. In: Proceedings of the 17th international congress on applications of lasers and electro-optics, ICALEO'98, 1998.

[3] Baufeld B, der Biest OV, Gault R. Additive manufacturing of Ti6Al4V components by shaped metal deposition: microstructure and mechanical properties. Mater Des 2010;31(Supplement 1):S106–S111.

[4] Santos EC, Shiomi M, Osakada K, Laoui T. Rapid manufacturing of metal components by laser forming. Int J Mach Tool Manuf 2006;46:1459–1468.

[5] Gibbons GJ, Hansell RG. Direct tool steel injection mould inserts through the arcam EBM free-form fabrication process. Assembly Autom 2005;25(4):300–305.

[6] Syed W, Pinkerton A, Li L. A comparative study of wire feeding and powder feeding in direct diode laser deposition for rapid prototyping. Appl Surf Sci 2005;247:268–276.

[7] J. Nurminen, Hot-wire laser cladding: process, materials and their properties, PhD thesis, Tampere University of Technology, Publication 765, 2008.

[8] Kim J-D, Peng Y. Plunging method for Nd: YAG laser cladding with wire feeding. Opt Laser Eng 2000;33(4):299–309.

[9] Moures F, Cicala E, Sallamand P, Grevey D, Vannes B, Ignat S. Optimisation of refractory coatings realised with cored wire addition using a high-power diode laser. Int J Mach Tool Manu 2005;200:2283–2292.

[10] Capello E, Colombo D, Previtali B. Repairing of sintered tools using laser cladding by wire. J Mater Process Technol 2005;164-165:990–1000.

[11] Syed W, Li L. Effects of wire feeding direction and location in multiple layer diode laser direct metal deposition. Appl Surf Sci 2005;248:518–524.

[12] Hussein N, Segal J, McCartney D, Pashby I. Microstructure formation in Waspaloy multilayer builds following direct metal deposition with laser and wire. Mater Sci Eng A 2008;497(1–2):260–269.

[13] Miranda R, Lopes G, Quintino L, Rodrigues J, Williams S. Rapid prototyping with high power fiber lasers. Mater Des 2008;29:2072–2075.

[14] Mok S, Bi G, Folkes J, Pashby I. Deposition of Ti6Al4V using a high power diode laser and wire, Part I: investigation on the process characteristics. Surf Coat Technol 2008;202:3933–3939.

[15] Mok S, Bi G, Folkes J, Pashby I, Segal J. Deposition of Ti6Al4V using a high power diode laser and wire, Part II: investigation on the mechanical properties. Surf Coat Technol 2008;202:4613–4619.

[16] Cao X, Jahazi M, Fournier J, Alain M. Optimization of bead spacing during laser cladding of ZE41A–T5 magnesium alloy castings. J Mater Process Technol 2008;205:322–331.

[17] Charles C, Järvstråt N. Modelling Ti6Al4V microstructure by evolution laws implemented as finite element subroutines: application to TIG metal deposition. In: Proceedings of the 8th international conference on trends in welding research, 2008, p. 477–85.

[18] Medrano A, Folkes J, Segal J, Pashby I. Fibre laser metal deposition with wire: parameters study and temperature monitoring system. In: Proceedings of the SPIE, vol. 7131, 2009, p. 713122.

[19] Brandl E, Baufeld B, Leyens C, Gault R. Additive manufactured Ti6Al4V using welding wire: comparison of laser and arc beam deposition and evaluation with respect to aerospace material specifications. Phys Proc 2010;5:595–606.

[20] Baufeld B, Brandl E, van der Biest O. Wire based additive layer manufacturing: comparison of microstructure and mechanical properties of Ti6Al4V components fabricated by laser-beam deposition and shaped metal deposition. J Mater Process Technol 2011; 211(6) :1146 –58, http://dx.doi.org/10.1016/j.jmatprotec.2011.01.018.

[21] Syed W, Pinkerton A, Li L. Combining wire and coaxial powder feeding in laser direct metal deposition for rapid prototyping. Appl Surf Sci 2006;252: 4803–4808.

[22] Wang F, Mei J, Wu X. Microstructure study of direct laser fabricated Ti alloys using powder and wire. Appl Surf Sci 2006;253:1424–1430.

[23] Wang F, Mei J, Jiang H, Wu X. Laser fabrication of Ti6Al4V/TiC composites using simultaneous powder and wire feed. Mater Sci Eng A 2007;445–446:461–466.

[24] Heralić A, Ottosson M, Hurtig K, Christiansson A-K. Visual feedback for operator interaction in robotized laser metal deposition. In: Proceedings of the 22nd international conference on surface modification technologies, 2008, p. 297–304.

[25] Heralić A, Christiansson A-K, Ottosson M, Lennartson B. Increased stability in laser metal wire deposition through feedback from optical measurements. Opt Laser Eng 2010;48(4):478–485.

[26] Hu D, Kovacevic R. Sensing, modeling and control for laser-based additive manufacturing. Int J Mach Tool Manuf 2003;43:51–60.

[27] Toyserkani E, Khajepour A. A mechatronic approach to laser powder deposition process. Mechatronics 2006;16:631–641.

[28] Iravani-Tabrizipour M, Toyserkani E. An image-based feature tracking algorithm for real-time measurement of clad height. Mach Vision Appl 2007;18: 343–354.

[29] Mazumder J, Dutta D, Kikuchi N, Ghosh A. Closed loop direct metal deposition: art to part. Opt Laser Eng 2000;34:397–414.

[30] Bi G, Gasser A, Wissenbach K, Drenker A, Poprawe R. Identification and qualification of temperature signal for monitoring and control in laser cladding. Opt Laser Eng 2006;44(12):1348–1359.

[31] Bi G, Gasser A, Wissenbach K, Drenker A, Poprawe R. Characterization of the process control for the direct laser metallic powder deposition. Surf Coat Technol 2006;201(6):2676–2683.

[32] Bi G, Schürmann B, Gasser A, Wissenbach K, Poprawe R. Development and qualification of a novel laser-cladding head with integrated sensors. Int J Mach Tool Manuf 2007;47:555–561.

[33] Tang L, Ruan J, Landers RG, Liou F. Variable powder flow rate control in laser metal deposition processes. J Manuf Sci Eng 2008;130(4):041016.

[34] Doubenskaia M, Bertrand P, Smurov I. Optical monitoring of Nd: YAG laser cladding. Thin Solid Films 2004;453-454:477–485.

[35] Hua T, Jing C, Xin L, Fengying Z, Weidong H. Research on molten pool temperature in the process of laser rapid forming. J Mater Process Technol 2008;198:454–462.

[36] Hua T, Jing C, Fengying Z, Xin L, Weidong H. Estimation of laser solid forming process based on temperature measurement. Opt Laser Technol 2010;42:47–54.

[37] Bristow D, Tharayil M, Alleyne A. A survey of iterative learning control. IEEE Control Systems Magazine 2006;26(3):96–114.

[38] Arimoto S, Kawamura S, Miyazaki F. Bettering operation of robots by learning. J Robotic Syst 1984;1(2):123–140.

[39] Craig JJ. Adaptive control of manipulators through repeated trials. In: Proceedings of the American Control Conference, vol. 3, 1984, p. 1566–73.

[40] Wallén J, Estimation-based iterative learning control. Dissertation No. 1358, Linköping University, Department of Electrical Engineering, Linköping, Sweden, 2011.

[41] Mitra SK. Digital signal processing. 2nd ed.McGraw-Hill; 2001.

[42] Goodwin G, Salgado M, Graebe S. Control system design. Upper Saddle River, NJ, London: Prentice Hall; 2001.

[43] Longman RW. Iterative learning control and repetitive control for engineering practice. Int J Control 2000;73(10):930–954.

[44] Norrlöf M, Gunnarsson S. Time and frequency domain convergence properties in iterative learning control. Int J Control 2002;75(14):1114–1126.